# Application of Rotating RF Coil Array in $B_1$ Shimming with Strict Local SAR Constraints

Jin Jin[1], Feng Liu[1], Adnan Trakic[1], Ewald Weber[1], and Stuart Crozier[1]
[1]*University of Queensland, St Lucia, Queensland, Australia*

***Introduction:*** The most challenging radiofrequency (RF)-related issues at high fields are the inhomogeneous excitation and high RF energy absorption, quantified as specific absorption rate (SAR). The former can lead to image intensity variation and regional signal drop-offs, while the latter raises concerns towards the safe use of high-field system. To date, $B_1$-shimming is one of the most promising techniques to circumvent these issues. However, it has been demonstrated that the number of independently controlled transmit elements necessary for applications at 7 T and above is potentially very large [1]. Massive parallel transmit arrays face challenges such as shallow RF penetration and difficulties in managing coil-coil couplings. Moreover, increasing the number of coils and individual power amplifiers escalates the operational cost and system complexity. Herein, we propose using a low channel-count rotating RF coil array [2, 3] to perform $B_1$-shimming, while the maximum 10-gram averaged SAR is strictly controlled.

***Methods:*** The rotating RF coil array (RRFCA) (Fig.1B) employed in this study consists of only 4 elements (denoted by 4 colours). In contrast to conventional phased array coils (PAC) (Fig.1A), which remain stationary, the RRFCA moves to various discrete locations (e.g. 15°, 30° … etc.) to transmit a pulse from each location. Therefore, higher degrees of freedom (DOFs) are achieved. From the example in Fig.1B, 24 complex voltages and 24 unique transmit profiles are used to optimise the $B_1$ profiles and regulate local SAR. When shimming with the stationary PAC, the combined $B_1$ and $E$ fields from all channels can be expressed using Eq.(1), where $W = [w_1 \ldots w_C]^T$ is the complex driving voltage of all C channels; ${}_c\boldsymbol{B}_1^+(r)$ and ${}_c\boldsymbol{E}(r)$ denote the complex $B_1$ and $E$ fields of the $c$-th channel at the $\boldsymbol{r}$-th sample location respectively. The local SAR averaged over a volume $V$ can therefore be expressed as Eq.(2) [4].

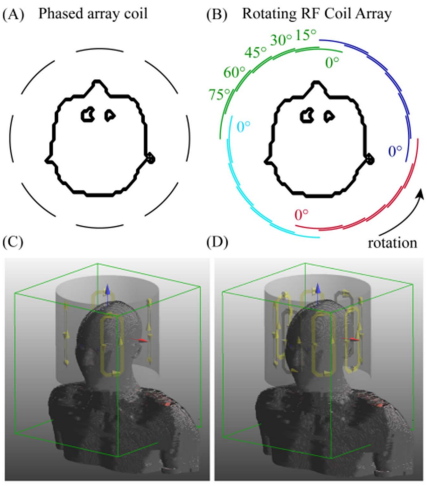

Fig.1 Illustration of the phased-array coil and rotating RF coil array

$$\begin{cases} \left(\overline{\boldsymbol{B}_1^+}\right)_r = [B_1]_r \cdot W \\ \overline{\boldsymbol{E}}_r = [\boldsymbol{E}]_r \cdot W \end{cases} \quad (1)$$

$$where \begin{cases} [B_1]_r = \left[ {}_1\boldsymbol{B}_1^+(r) \ \cdots \ {}_C\boldsymbol{B}_1^+(r) \right] \\ [\boldsymbol{E}]_r = \left[ {}_1\boldsymbol{E}(r) \ \cdots \ {}_C\boldsymbol{E}(r) \right] \end{cases}$$

$$SAR(r) = \frac{1}{V}\int_{r\in V} \frac{\sigma(r)}{\rho(r)} \left|\overline{\boldsymbol{E}_r}\right|^2 dV = W^H Q_r W, \quad (2)$$

$$Q_r = \frac{1}{V}\int_{r\in V} \frac{\sigma(r)}{\rho(r)} \left(\overline{\boldsymbol{S}_r}\right)^H \left(\overline{\boldsymbol{S}_r}\right) dV$$

$$\left|\left(\overline{\boldsymbol{B}_1^+}\right)_r\right| = \sum_{p=1}^{P} \left|[B_1]_r^p \cdot W^p\right| \quad (3)$$

With the RRFCA however, the electromagnetic fields interact in a different fashion. At each angular position, the $E$ and $H$ fields of the individual channels interact with each other as PAC does, giving rise to combined fields, as shown in Eq.(1). However, such interactions do not occur between fields of different locations (and times). Ignoring $T_1$ relaxation, the combined $B_1$ field magnitude and SAR distribution of RRFCA are therefore shown in Eqs.(3) and (4), respectively. The adapted vector $W'$ is derived from concatenating all $W^p$ vectors ($p$ = 1, 2 … $P$, denotes the angular positions the RRFCA visits), whereas the new matrix $Q'$ is block diagonal, combining all $Q^p$ matrices. For both PAC and RRFCA techniques, the optimal coil driving combination ($W$ or $W'$) can be obtained by solving Eq.(5). The number of SAR constraints is typically in the order of hundreds of thousands (100,000's). $Q$ matrix compression techniques [5] were employed to dramatically reduce the number of constraints to several hundreds (100's), facilitating efficient numerical optimisation. Active set algorithm implemented in Matlab (Mathworks) optimisation toolbox is employed to solve the quadratic constrained problem in the form of Eq.(5). To circumvent local minima, each optimisation was repeated 50 times with randomly generated initial estimates.

$$SAR(r) = (W')^H Q_r' W',$$

$$W' = \begin{bmatrix} W^1 \\ \vdots \\ W^P \end{bmatrix}, Q_r' = \begin{bmatrix} Q_r^1 & & \\ & \ddots & \\ & & Q_r^P \end{bmatrix}_r \quad (4)$$

$$\min_W \left\| \sum_{ROI} \left( \left|\left(\overline{\boldsymbol{B}_1^+}\right)_r\right| - (B_1)_{des} \right) \right\|_2^2 \quad (5)$$

$$s.t.: W^H Q_r W \le SAR_{Limit}, \forall \boldsymbol{r}$$

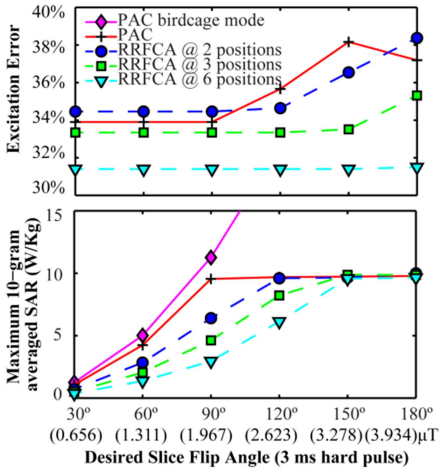

Fig.2 $B_1$ excitation error and maximum 10-gram SAR

In this work, an 8-element PAC (Fig.1C) and 4-element RRFCA (Fig.1D) were modelled numerically for 7 T applications (298.2 MHz). Both coil models have the same overall size ($\phi_{coil\_former}$ = 230 mm, $\phi_{shield}$ = 280 mm) and element dimension (65 × 180 mm). Such coil configurations provided channel isolation of no less than 15 dB and 33 dB for the PAC and RRFCA, respectively. Both PAC and RRFCA setups were loaded with anatomically accurate human model (NORMAN [6]), with linear voxel resolution ranging from 1.7 mm to 3.6 mm depending on the coil model. As can be seen, the body model was truncated below 450 mm from the top of the head to facilitate more efficient computation while providing correct loading to the RF coil. The complete models contain approximately 4.6 to 9.7 million cells including perfectly matched layers. The 4-element RRFCA was modelled at various angular locations, as shown in Fig.1B. The effects of using 2 positions (0° and 45°), 3 positions (0°, 30° and 60°) and all 6 positions were compared. The electromagnetic modelling and calculation is assisted with commercially available software package SEMCAD X (SPEAG, Zurich, Switzerland). The shimming of the $B_1$ fields was performed over the entire axial slice of 7 cm from the top of the head. The local 10 gram averaged SAR was constrained to 10 W/Kg.

***Results and Discussion:*** The excitation error of the transmit $B_1$ filed magnitude, defined as the standard deviation divided by the mean [4], is shown in Fig.2. It can be seen from the maximum 10-g SAR values (Fig.2, bottom), without SAR-constrained optimisation, that the birdcage excitation mode exceeded the max 10-g limit when a 90° pulse was applied. With optimisation, the PAC actuated SAR constraints with 90° excitation, whereas the RRFCA did not activate SAR constraint until higher desired flip angles (i.e. 120°, 150° and 180° for 2, 3 and 6 angular positions respectively). It is noted that the local SAR limit of 10 W/Kg was strictly maintained in all cases. Comparing the 4-channel RRFCA of 2 positions with the 8-channel PCA, it appeared that they had similar excitation accuracy (Fig.2, top). Close examination reveals, however, that the PAC failed to achieve the desired flip angle due to the strong SAR constraints, as apparent from Fig.3. Being able to distribute RF energy spatially in more than one pulse, RRFCA was able to achieve better excitation with the same set of spatial transmit profiles. This indicated the benefit of exploiting the time-domain DOFs in RF shimming [7]. Figs.2 and 3 also show that, when more spatial and temporal DOFs are available, the RRFCA with 3 and 6 positions achieved even more homogeneous $B_1$ profiles. Higher performance of RRFCA can be expected by optimising the element penetration and decoupling (currently 33 dB).

***Conclusion:*** In this work, the feasibility of employing a rotating RF coil array for mitigating $B_1$ inhomogeneity while strictly enforcing local SAR limit is investigated. By providing a large number of transmit sensitivity profiles and partitioning the RF pulsing process in the temporal domain, RRFCA was able to successfully homogenise $B_1$ fields in a 2D slice whilst maintaining the local SAR limit in the whole head model at 7 T.

[1]. Mao, W.et al. MRM, 2006. 56(4): p. 918-922. [2]. Trakic, A., et al., Concepts in MR. B. 2009. 35B(2): p. 59-66. [3]. Trakic, A., et al., JMR, 2009. 201(2): p. 186-198. [4]. Homann, H., et al., MRM, 2012. 25(3): p. 193-204. [5]. Eichfelder, G. and M. Gebhardt, MRM, 2011. 66(5): p. 1468-1476. [6]. Dimbylow, P.J., PMB, 1997. 42(3): p. 479. [7] Collins CM, et al. MRM. 2007. 57(3): p. 470-474.

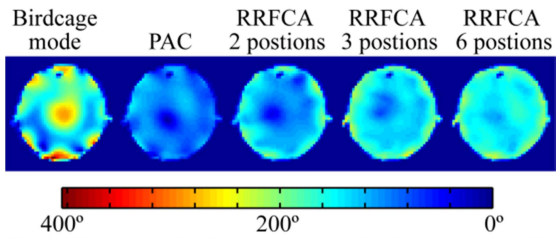

Fig.3 Flip angle distribution with excitation target of 180°